JOURNAL OF AIRCRAFT
Vol. 34, No. 5, September–October 1997

Dual-Point Design of Transonic Airfoils Using the Hybrid Inverse Optimization Method

Hyoung-Jin Kim* and Oh-Hyun Rho†
Seoul National University, Seoul 151-742, Republic of Korea

A new dual-point design procedure has been developed to improve the aerodynamic performance of transonic airfoils at two design points. A target pressure distribution at each design point was optimized by a genetic algorithm. Single-point design was performed to make an airfoil that produced given target pressures and satisfied specified geometric constraints at each design point. Following this, several intermediate airfoils were made by the hybrid inverse optimization method. A redesigned airfoil of dual-point design was found using the weighted average of intermediate airfoil shapes, based on the linear variation assumption. Two examples of dual-point design to improve the performance at an off-design condition are presented. These design examples show that the dual-point design procedure presented in this paper is very efficient for the multipoint design of transonic airfoils.

Nomenclature

C_l, C_d, C_{dw}	=	lift, drag, and wave drag coefficient
C_{pt}, C_{pc}	=	target and computed pressure coefficient
c	=	airfoil chord
M, M_∞	=	local, freestream Mach number
Rn	=	noise radius
t	=	airfoil maximum thickness
w	=	weighting factor
Δy	=	vertical displacement of airfoil surface point

Subscripts

i	=	index of airfoil surface grid points
0	=	value of RAE2822
1, 2	=	first and second design point

Introduction

IN the aerodynamic design of transonic airfoils, drag was greatly reduced at the design point by using single-point designs. However, such airfoils often showed poor performance in off-design conditions. Aerodynamic performance may be improved if a dual-point design procedure can be performed for the consideration of two design conditions. Dual-point design procedures using direct numerical optimization have already been demonstrated.[1] The number of geometric airfoil configurations evaluated in the dual-point design process in Ref. 1 ranged from 61 to 105. Too much computational time was required, therefore, when compared with that of the inverse method by Mineck et al.,[2] which requires about six analysis cases and two design cases to be run.

Alternative dual-point design procedures using an inverse design method were applied for transonic airfoil design by Mineck et al.[2] They used two procedures: airfoil shape averaging and target pressure averaging, with an assumption that aerodynamic properties vary linearly with the weighting factor of airfoil shape averaging. It was found that the former was better for the specified design problem.

Received Nov. 17, 1996, presented as Paper 97-0512 at the AIAA 35th Aerospace Sciences Meeting, Reno, NV, Jan. 6–9, 1997; revision received April 5, 1997; accepted for publication April 9, 1997.

*Graduate Research Assistant, Department of Aerospace Engineering. Student Member AIAA.

†Professor, Department of Aerospace Engineering. Senior Member AIAA.

The objective of the present study was to demonstrate a new dual-point design procedure for transonic airfoils using the hybrid inverse optimization method.[3] A new objective function was defined by the author utilizing the versatility of the hybrid inverse optimization method. For the specification of the target pressure at each design point, an existing target pressure optimization code[4] was used with a genetic algorithm (GA) (Ref. 5).

This paper will present some details of the procedure used in the dual-point design, and some examples of Mach design and α design. The dual-point design results will be compared with those of the single-point design.

Flow Analysis

An existing two-dimensional Navier–Stokes solver developed by Hwang[6] was used for flow analysis. A Reynolds-averaged two-dimensional compressible Navier–Stokes equation was used in conservation form. Roe's flux difference splitting (FDS) scheme was adopted for the space discretization; the MUSCL approach with flux limiter was employed to obtain higher-order accuracy. Beam and Warming's alternating direction implicit (ADI) method was used in the implicit part. Turbulence effects were considered using the Baldwin–Lomax model with relaxation technique. To improve convergence, local time stepping was applied. A C-type grid system around the airfoil was generated by a conformal mapping technique. We used 135 points in the chordwise direction, 41 points in the normal direction, and 95 points on the airfoil surface.

To validate this flow solver, the flowfield around the RAE2822 airfoil was analyzed with a flow condition of $M_\infty = 0.730$, $\alpha = 2.79$ deg, and $Re = 6.5 \times 10^6$.

Figure 1 shows the surface pressure distribution of flow analysis and the experimental result.[7] The computed pressure compares well with the experimental data, with the exception of the shock strength, which was overestimated. In Table 1, analyzed lift coefficient is in good agreement with measured value; however, drag is overestimated (as in Ref. 8).

Hybrid Inverse Optimization Method

An auxiliary ordinary differential equation [modified Garabedian-McFadden (MGM) equation[9]] was used to correlate the difference between the computed surface and target pressures to modify the airfoil geometry:

$$F_0\Delta y + F_1\Delta y_x + F_2\Delta y_{xx} = R, \qquad (R = C_{pt} - C_{pc}) \quad (1)$$

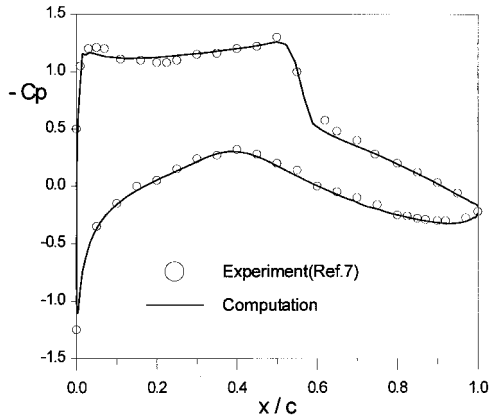

Fig. 1 Comparison of computed and measured surface pressure distribution.

where coefficients F_0, F_1, and F_2 are nonnegative constants chosen to provide a stable iterative process, and R is the residual. The MGM equation is solved using a finite difference scheme. A typical equation evaluated at the ith surface grid point is

$$A_i\Delta y_{i+1} + B_i\Delta_{yi} + C_i\Delta y_{i-1} = R_i \tag{2}$$

The detailed expressions for coefficients A_i, B_i, and C_i are given by Malone et al.[9] The algebraic equations [Eq. (2)] forms a tridiagonal system and can be written as

$$[M]\{\overline{\Delta \mathbf{y}}\} = \{\mathbf{R}\} \tag{3}$$

The objective function is defined to solve Eq. (3) with an optimization technique, as follows:

$$F(\overline{\Delta y}) = \tfrac{1}{2}\left|[M]\{\overline{\Delta \mathbf{y}}\} - \{\mathbf{R}\}\right|^2 \tag{4}$$

The gradient of the objective function is given by

$$\nabla F(\overline{\Delta y}) = [M]^T([M]\{\overline{\Delta \mathbf{y}}\} - \{\mathbf{R}\}) \tag{5}$$

A penalty function method was used to specify the geometric constraint. The objective function [Eq. (4)] was modified by adding the penalty function term, as follows:

$$\Phi(\overline{\Delta y_i}) = F(\overline{\Delta y_i}) + r_p P(\overline{\Delta y_i}) \tag{6}$$

where $P(\overline{\Delta y_i})$ is the penalty function and r_p is the multiplier. The solution of the system of Eq. (2) can be obtained by finding a vector $\{\overline{\Delta \mathbf{y}}\}$ that minimizes the objective function [Eq. (6)]. The conjugate gradient method[10] is used to minimize the objective function [Eq. (6)]. The computational time required to calculate the objective function and its derivative is negligible compared with the time required by the flow solver.

The previous method was developed by Santos et al.,[3] and is referred to as the hybrid inverse optimization method because it solves the inverse design problem with the optimization technique.

Dual-Point Design Procedure

To perform dual-point design, we defined a new objective function that averages the two objective functions of two design points, as follows:

$$F(\overline{\Delta y}) = \frac{w}{2}\left|[M_1]\{\overline{\Delta \mathbf{y}}\} - \{\mathbf{R}_1\}\right|^2 + \frac{1-w}{2}\left|[M_2]\{\overline{\Delta \mathbf{y}}\} - \{\mathbf{R}_2\}\right|^2 \tag{7}$$

Table 1 Comparison of measured and predicted aerodynamic coefficients

	C_l	C_d	C_m
Experiment[7]	0.803	0.0168	−0.099
Numerical result[8] (B-L model)	0.7950	0.01884	−0.09513
Numerical result (current solver)	0.7971	0.01892	−0.09592

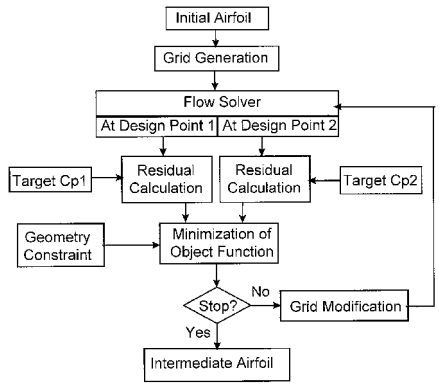

Fig. 2 Flowchart of DTAD routine for single-point design.

Figure 2 shows the flowchart of the dual-point transonic airfoil design (DTAD) routine. First, a baseline airfoil is selected, and a grid system is generated around the airfoil. The surface pressure is obtained from the flow solver at each design point. The hybrid inverse optimization method is used to obtain vertical displacements of airfoil surface grid points reducing the objective function [Eq. (7)] and satisfying the geometric constraints. The grid system is then modified algebraically for the new airfoil. This design cycle is repeated until the airfoil modification is sufficiently small.

If w is 1 or 0, Eq. (7) comes to Eq. (4), and the DTAD routine becomes the routine for single-point design, which is referred to as the TAD (transonic airfoil design) routine.[4]

To find a vector $\{\overline{\Delta \mathbf{y}}\}$ that minimizes the objective function of Eq. (7) is to find an airfoil that gives a surface pressure distribution as close to the target pressure as possible at both design points. It is expected that the DTAD routine will produce better airfoils than those designed simply by averaging the airfoil shape or target pressure.[2] There is no guarantee, however, that the output airfoil from the DTAD routine would be subject to design constraints such as the C_l constraint. Thus, the output airfoil is only used as the intermediate airfoil, and the optimum airfoil is sought in the design space of intermediate airfoils. To find the optimum airfoil efficiently, it is assumed that the aerodynamic coefficients such as C_l and C_d vary linearly with the weighting factor of airfoil shape averaging. This assumption was made by Mineck et al.,[2] and found to be reasonable for two sufficiently close design points. This assumption will be referred to hereafter as the linear variation assumption (LVA). The accuracy of this assumption is improved by adding the even-weight averaged airfoil of the two single-point designed airfoils as another intermediate airfoil.

The dual-point design procedure suggested in this study begins with optimizing target pressures at each design point. A single-point design is performed with the optimized target pressure at each design point by the TAD routine. The two designed airfoils are then analyzed at the other design point. Then the DTAD routine is run several times, changing the value of w to produce intermediate airfoils. In this study, five values of w were used: 0.1, 0.3, 0.5, 0.7, and 0.9. There are now eight intermediate airfoils; two single-point designed airfoils by TAD, one even-weight averaged airfoil of the two, and five airfoils produced by the DTAD routine with five weighting factors.

The design space is inside the convex polygon made of the aerodynamic coefficients of intermediate airfoils in the w vs C_l and w vs C_d graphs. To find the optimum airfoil in the design space, linearly interpolated aerodynamic coefficients are obtained by applying the LVA to three airfoils selected from the eight intermediate airfoils. The process is repeated for every possible combination of three airfoils of the eight intermediate airfoils. If the optimum airfoil is not subject to the imposed constraints or needs to be improved, the target pressure at one design point is modified or reproduced with some variation of the C_l and/or the C_d value. Then the TAD and DTAD routine is run again to produce supplementary intermediate airfoils and the previously mentioned searching procedure is repeated. However, only one dual-point design cycle was required to obtain satisfactory results in all design examples studied here. If the optimum airfoil is found to be satisfactory, the shape of the optimum airfoil is constructed from the linear combination of three base intermediate airfoils with Eq. (8), and then analyzed at both design points to ascertain the predicted aerodynamic coefficients:

$$y_i = \sum_{j=1}^{N} w_j y_{ij}, \qquad \sum_{j=1}^{N} w_j = 1 \tag{8}$$

One cycle of the dual-point design procedure requires four analysis cases, two runs of TAD and five runs of DTAD. The TAD routine requires less than 1.5 times the cost of an analysis, and the DTAD routine requires less than 2.5 times the cost of an analysis. Thus, one complete cycle of the dual-point design procedure requires less than 20 times the cost of an analysis. This is a much smaller computational load compared with that of Hager et al.,[1] where the flow solver was run more than 60 times for the direct numerical optimization. If the smaller number of w is used for the DTAD routine, the computational time for a dual-point design can be reduced. However, this reduces the area of the design space, and may result in the failure to find the optimum airfoil in the design space of intermediate airfoils.

Optimization of Target Pressure

A target pressure optimization code for the optimization of target pressures for transonic airfoil inverse design has been developed by the authors.[4] Figure 3 shows the characteristic surface pressure distribution for transonic airfoils defined by eight points. Shape functions are used for interpolation between these points. The location of characteristic points, local Mach number at each point, and the coefficients of shape functions are used as design variables. Shape functions, defined by van Egmond,[11] were partially used, and a few shape functions were redefined for simplicity and efficiency. The boundary-layer calculation was avoided to reduce computational time. Instead, the slope of the pressure distribution was checked as the flow separation criteria. Some details are shown here for completeness.

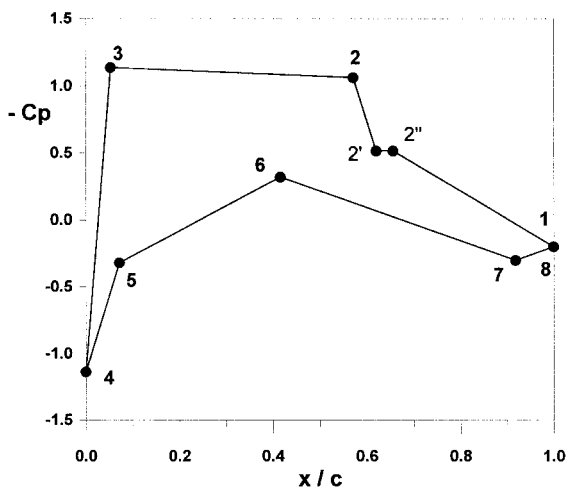

Fig. 3 Schematic representation of target pressure.

Stagnation Flow Region (4–3, 4–5)

We used a stagnation flow shape function,[11] defined by approximating the potential flow velocity distribution around elliptic cylinders (for small x/c and small incidence angle):

$$\frac{u}{u_\infty} = \frac{(1 + da_1)\sqrt{da_3 \cdot \frac{x}{c}} \pm \left[da_2 + da_3 \cdot da_4 \cdot \frac{x}{c}\right]\sqrt{1 - da_3 \cdot \frac{x}{c}}}{\sqrt{da_3 \cdot \frac{x}{c} + \frac{1}{4} da_1^2}} \tag{9}$$

(+ sign for upper surface and − sign for lower surface). da_1–da_4 represent the design variables that should be adjusted by the optimization procedure. Nose radius and incidence angle may be estimated from

$$(R/c)_{\text{nose}} = (0.5/da_3) \cdot da_1^2 (1 - M_\infty^2), \quad \alpha = da_2 \cdot \sqrt{(1 - M_\infty^2)}\ (\text{rad})$$

Rooftop Region (3–2, 5–6)

$$M = db_1 + db_2[(x/c) - (x/c)_{b_0}]^{1 + db_3} \tag{10}$$

Index b_0 refers to the starting point of the region.

Shock Relation (2–2′)

Shock wave is specified when M exceeds 1.1 at control point 2. The shock thickness value was set to $0.05c$. In viscous airfoil flow, the pressure jump measured at the foot of the shock is less than the Rankine–Hugoniot pressure jump. A modified Rankine–Hugoniot relation of the following form was used for an approximation of pressure jump[12]:

$$\frac{p_2}{p_2} = 1 + \frac{2\gamma}{\gamma + 1} A(M_2^2 - 1), \qquad 0.55 < A < 0.75 \tag{11}$$

Here, the range of the A value is determined from experimental data in Ref. 12, and here, A is set to 0.65.

Constant Pressure Region Behind Shock (2′–2″)

It is known that a pressure plateau behind the shock wave is necessary to stabilize the boundary layer.[13] A constant pressure distribution is specified for length l, l being the design variable. However, it is not intended to stabilize the boundary layer by varying l.

Pressure Recovery Region on Upper Surface (2″–1)

This region might be represented by an approximating function of Stratford pressure distribution. A straight line connecting two points was used for simplicity. C_p at the trailing edge is set to 0.2.

Pressure Recovery Region on Lower Surface (6–7)

A fourth-order polynomial is defined for this region as

$$M = M_6 + dc_1\left(\frac{x}{c} - \frac{x_6}{c}\right) + dc_2\left(\frac{x}{c} - \frac{x_6}{c}\right)^2 + dc_3\left(\frac{x}{c} - \frac{x_6}{c}\right)^3 + dc_4\left(\frac{x}{c} - \frac{x_6}{c}\right)^4 \tag{12}$$

Rear Loading Region (7–8)

For this region a simple polynomial is defined as

$$M = M_7 + dd_1\left(\frac{x}{c} - \frac{x_7}{c}\right) + dd_2\left(\frac{x}{c} - \frac{x_7}{c}\right)^2 \tag{13}$$

Characteristic points and shape functions presented previously can represent target pressure distribution around the transonic airfoil. Not all of them are independent, and 15 design variables were used for optimization of the target pressure distribution.

An approximation of the maximum airfoil thickness is obtained by the following equation[11]:

$$\left(\frac{t}{c}\right) \cong -\frac{\sqrt{1-M_\infty^2}}{2}\int_0^1 \frac{(Cp_u + Cp_l)}{2}\, d\left(\frac{x}{c}\right) \qquad (14)$$

However, Eq. (14) does not consider effects of incidence angle, and was found to give deviated value from the exact one for various range of Mach numbers and incidence angle. Here, it was assumed that airfoils with the same value of Eq. (14) at given flow conditions have the same maximum thickness. The approximated maximum thickness value of baseline airfoil that is calculated with Eq. (14) was used as the input value for the maximum thickness in the target pressure optimization.

A relation to estimate the magnitude of wave drag has been proposed by Campbell[14]:

$$Cd_w \cong [0.04/(t/c)^{1.5}](M_2 - 1)^4 \qquad (15)$$

The objective function of this optimization problem is severely nonlinear, and even discontinuous.[11] Thus, a robust optimization technique that does not use the gradient information of the objective function should be used.

A GA is a searching algorithm based on natural selection and survival of the fittest. It has become popular recently because of its robustness and capability for finding the global minimum. In this study, the Genocop code,[5] which uses a GA, was applied for target pressure optimization.

Results and Discussion

All design examples were performed on the RAE2822 airfoil. The primary design point was $M_1 = 0.730$, $\alpha = 2.7$ deg, and $Re = 7 \times 10^6$.

Mach Design

The first design example was performed with a Mach number variation for the secondary design point. The secondary design point was selected as $M_2 = 0.710$ with other conditions unchanged.

The target pressure at the primary design point was optimized by GA. The objective of this optimization was to obtain a target pressure that has less wave drag than RAE2822, with lift, nose radius, and maximum thickness being almost the same. To obtain the optimal target pressure, the optimization problem was defined as

$$\begin{aligned}
&\text{minimize} && C_{dw}\\
&\text{subject to} && 1)\ C_{l0} - 0.002 \le C_l \le C_{l0} + 0.002\\
&&& 2)\ t_0 - 0.001 \le t \le t_0 + 0.003\\
&&& 3)\ C_{m0} - 0.02 \le C_m \le C_{m0} + 0.02\\
&&& 4)\ Rn = Rn_0\\
&&& 5)\ \frac{dCp}{dx} \le 2.3 \quad \text{(for the region behind the shock)}
\end{aligned} \qquad (16)$$

The fifth constraint on the slope of the pressure is taken from Ref. 13 to avoid flow separation after shock. Some other constraints were also imposed to make a reasonable and possible pressure distribution:

$$6)\ 0.4 \le Cp_7 \le Cp_8$$

$$7)\ Cp|_{x=0.2} \le 0$$

$$8)\ Cp|_{x=0.6} \le 0$$

$$9)\ -0.4 \le Cp_6 \le 0$$

where the subscripts are the control point numbers in Fig. 3. All of the constraints were included in the objective function as the penalty function term with proper weighting factors. GA was run with the population number of 200 and maximum

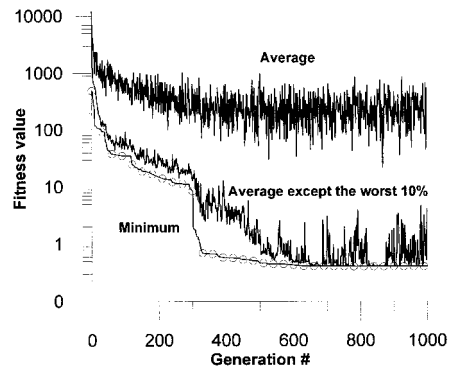

Fig. 4 Evolution of populations in target optimization.

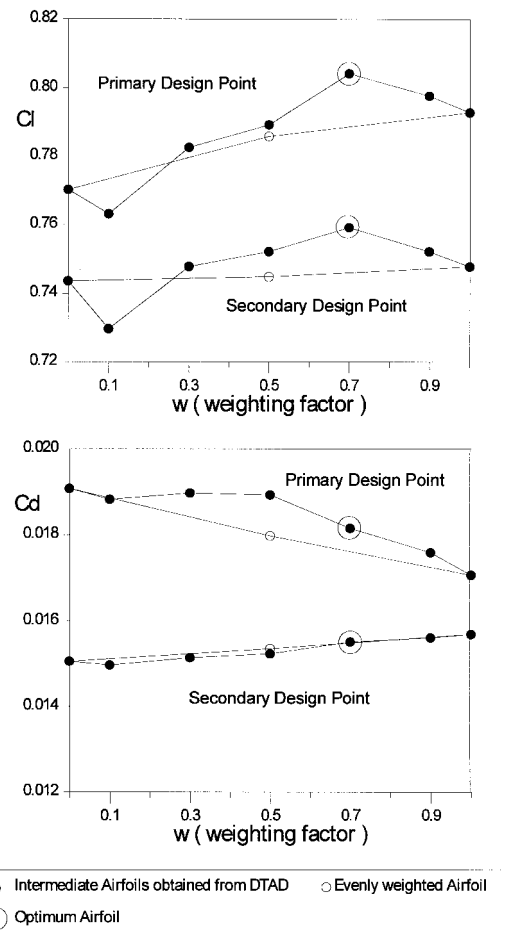

Fig. 5 Aerodynamic properties of intermediate and designed airfoils (Mach design): $M_1 = 0.730$, $M_2 = 0.710$, $\alpha = 1.7$ deg, and $Re = 7 \times 10^6$.

Table 2 Comparison of baseline and designed airfoils (Mach design)

	Primary design point			Secondary design point			t_{max}	
	C_l	C_d	C_m	C_l	C_d	C_m	%	Area
Baseline (RAE2822)	0.7796	0.01945	−0.09670	0.7452	0.01533	−0.08839	12.1	0.0778
1-point design	0.7929	0.01706	−0.09974	0.7478	0.01570	−0.09460	12.2	0.0790
Mach design	0.8043	0.01815	−0.1009	0.7593	0.01552	−0.09308	12.2	0.0790

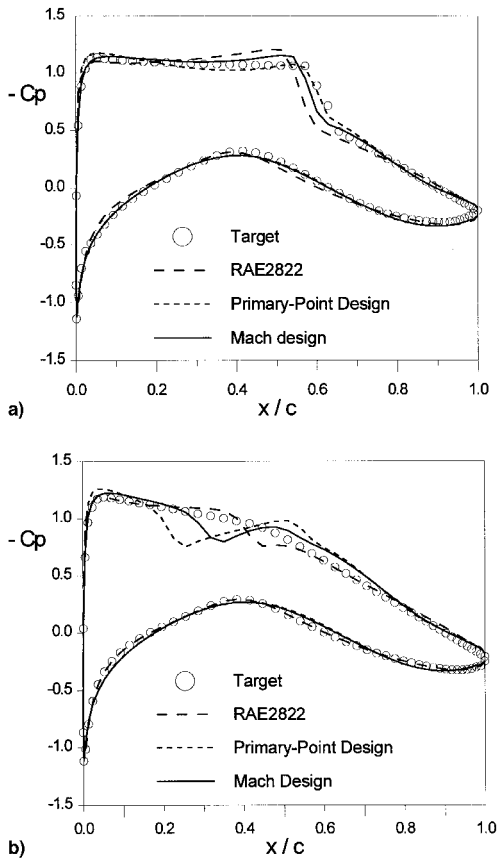

Fig. 6 Results of dual-point Mach design: surface pressure comparison at a) primary design point ($M_1 = 0.730$), and b) secondary design point ($M_2 = 0.710$).

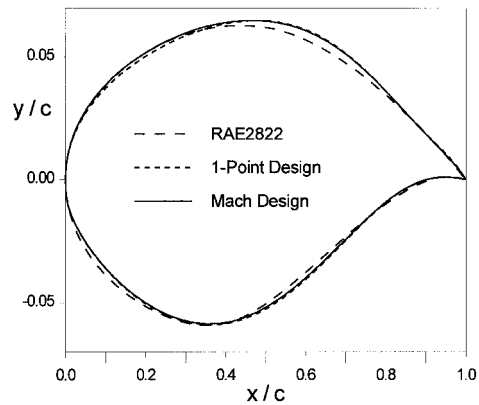

Fig. 7 Mach design: airfoil geometry comparison.

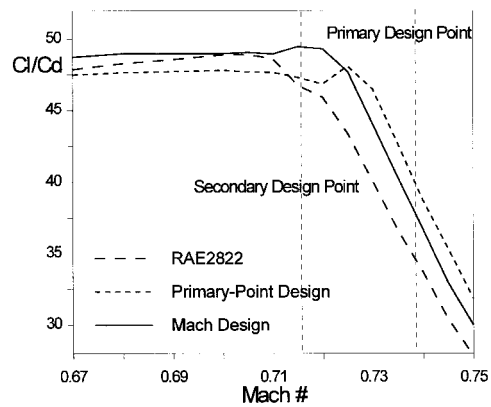

Fig. 8 Mach design: off-design performance at α = 2.7 deg.

generation number of 1000. Computational time for target optimization with GA was less than 10 min, using a Pentium personal computer running at 120 MHz. Figure 4 shows the convergence history of the objective function value with increasing generation numbers. The minimum fitness value converges in a stepwise manner, but the average value oscillates and does not converge to a specific value. This is because of the severe nonlinearity of the objective function. Average fitness values, except the worst 10% of populations, are almost the same order with the minimum value.

The target pressure at the secondary design point was also optimized with the optimization problem [Eq. (16)]. With a target pressure at each design point, eight intermediate airfoils were produced from the TAD and DTAD routines, and airfoil shape averaging. Area constraint was specified in the TAD and DTAD routines as

$$0.078 \leq \text{airfoil area} \leq 0.079 \tag{17}$$

The area constraint was specified to keep the airfoils similar. Other geometric constraints such as maximum thickness and nose radius constraints can also be considered in the TAD and DTAD routines. However, those were specified only in the target pressure generation level, and not in the inverse design code.

The weight-averaged airfoils then naturally satisfied the area constraint, but not necessarily the thickness and nose radius constraints. Figure 5 shows lift and drag (L/D) coefficients of these intermediate airfoils. The values of $w = 1$ and 0 represent the primary-point designed airfoil and the secondary-point designed airfoil, respectively. Here, the design problem for searching the optimum was defined as

$$\begin{aligned} \text{maximize} \quad & (C_l/C_d)_1 + (C_l/C_d)_2 \\ \text{subject to} \quad & C_{11} \geq C_{101} \\ & C_{102} \geq C_{102} \end{aligned} \tag{18}$$

The design space is inside the convex polygon of the intermediate airfoils in Fig. 5. With LVA, the optimum airfoil was sought in the design space. In this case the intermediate airfoil produced by the DTAD routine with $w = 0.7$, which is a vertex of the polygon, was found to be the optimum airfoil of the defined design problem. Figure 6 shows surface pressure distribution of the designed airfoil at two design points. Shock

Table 3 Comparison of baseline and designed airfoils (α design)

	Primary design point			Secondary design point			t_{max}	
	C_l	C_d	C_m	C_l	C_d	C_m	%	Area
Baseline (RAE2822)	0.7796	0.01945	−0.09670	0.6045	0.01345	−0.09689	12.1	0.0778
1-point design	0.7929	0.01706	−0.09974	0.6087	0.01419	−0.1048	12.2	0.0790
α design	0.8099	0.01758	−0.1038	0.6269	0.01388	−0.1078	12.2	0.0790

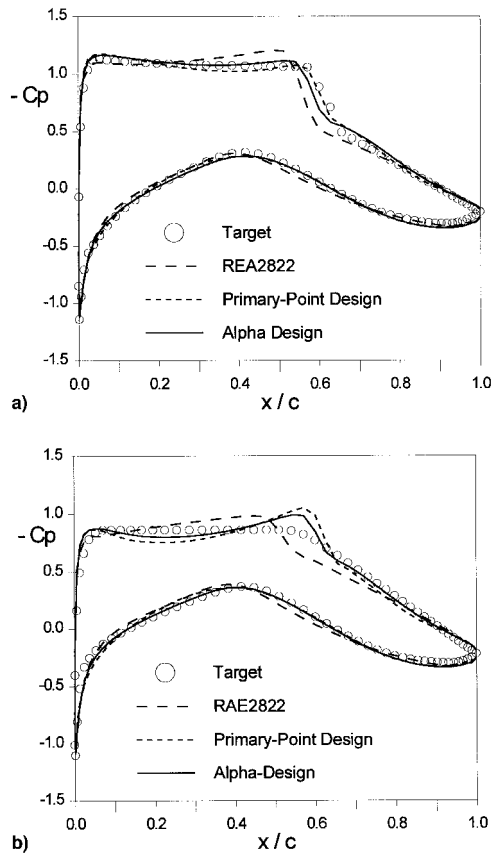

Fig. 9 Results of dual-point α design: surface pressure comparison at a) primary design point (α_1 = 2.7 deg), and b) secondary design point (α_2 = 1.7 deg).

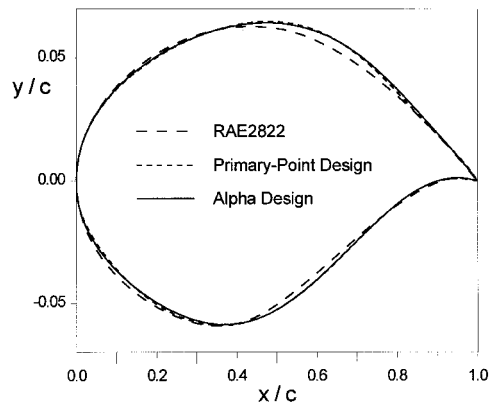

Fig. 10 α design: airfoil geometry comparison.

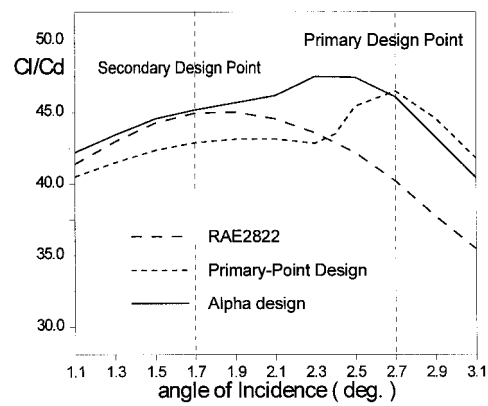

Fig. 11 α design: off-design performance at M = 0.730.

strength of the two-point designed airfoil is stronger at the primary point and weaker at the secondary point than the primary-point designed airfoil. Figure 7 shows the airfoil contours of the baseline and designed airfoil. Table 2, which compares baseline and designed airfoils, shows that the constraints on aerodynamic coefficients and contour area are exactly satisfied. It can also be noted that the maximum thickness constraint that was specified in the target pressure optimization level was also satisfied. The data on the nose radius constraint were not presented here. However, it is evident from Fig. 7 that baseline and designed airfoils have almost the same value of nose radius.

Figure 8 shows off-design performance of the designed airfoils. The *L*/*D* value of the primary-point designed airfoil is increased at the primary design point, but reduced at the secondary design point. The *L*/*D* value has remarkably been enhanced at the flow condition range between the two design points.

α Design

The second design case was performed with an α variation for the secondary design point. The secondary design point was selected as α_2 = 1.7 deg with other conditions unchanged from the primary design point. The target pressure of the primary design point was unchanged. The target pressure at the secondary design point was optimized with the optimization problem [Eq. (16)]. The same procedure as the first design case was performed with the area constraint of Eq. (17). Eight intermediate airfoils were produced as in the previous design case. In this case the design problem is defined as

$$\begin{aligned} &\text{minimize} && C_{d1} + C_{d2} \\ &\text{subject to} && C_{11} \geq C_{101} \\ & && C_{12} \geq C_{102} \end{aligned} \tag{19}$$

The optimum airfoil was sought in the design space using the linear variation assumption. In this case, the optimum airfoil that has the minimum value of summation of drag coefficient was found to be the primary-point designed airfoil. This is because the primary-point designed airfoil has much less drag than any other intermediate airfoils. However, the purpose of dual-point design is to improve the performance of off-design conditions. Thus, the objective function in Eq. (19) was modified to minimize the weighted summation of drag, instead of even weight summation. Here, the weight of 0.3 was put on the drag at the primary point, and the weight of 0.7 on the drag at the secondary point; a new optimum airfoil was found in the design space.

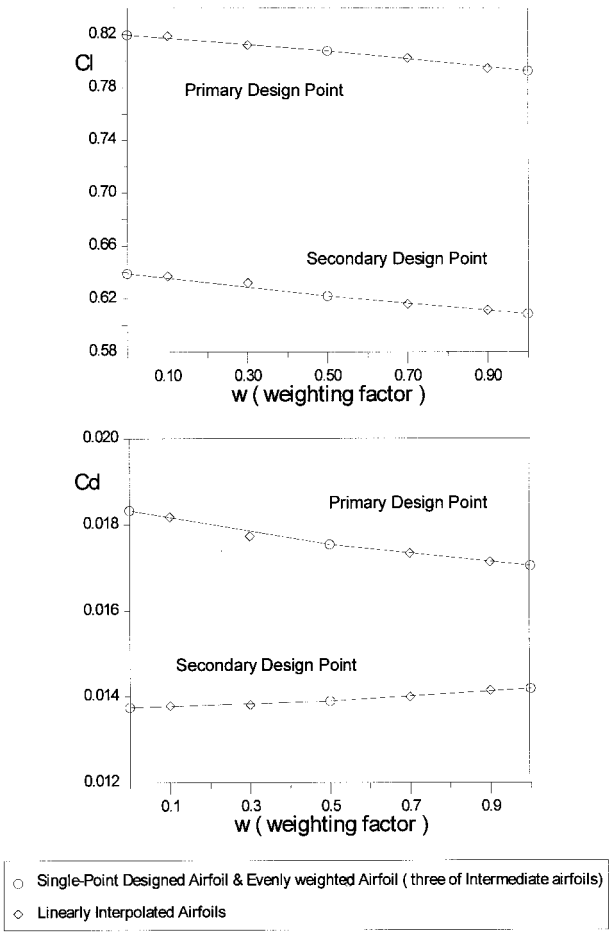

Fig. 12 Validation of linear variation assumption: α-design case.

The optimum airfoil C_l and C_d values predicted by the LVA and analyzed by a flow solver are marked by triangles.

Figure 9 shows surface pressure distribution of the designed airfoil at two design points. As in the Mach design case, shock strength of the two-point designed airfoil is stronger at the primary point and weaker at the secondary point than the primary-point designed airfoil. Figure 10 compares the airfoil contours of the baseline and designed airfoil. Table 3 shows that the constraints on aerodynamic coefficients and the contour area are exactly satisfied. The maximum thickness constraint that was specified in the target pressure optimization level was also satisfied.

Figure 11 shows off-design performance of the designed airfoil. Using the dual-point design, the *L/D* value at incidence angles lower than 2.7 deg were remarkably increased compared with the single-point designed airfoil.

Validation of the LVA

To validate the LVA again, airfoils linearly interpolated by Eq. (8) from the two single-point designed airfoils were analyzed by the flow solver. Figure 12 shows the results for the α design case. The solid line represents a line connecting w = 0 and w = 0.5, and a line connecting w = 0.5 and w = 1. Analyzed values compare well with the solid line. The same calculation was conducted for the Mach design case, and a similar result was obtained.

These results suggest that the LVA on the aerodynamic properties of the weight-averaged airfoil is reasonable, and that it is very efficient for finding the optimum airfoil in the design space of intermediate airfoils without any flow analysis.

Concluding Remarks

A new dual-point design procedure has been developed. The hybrid inverse optimization method has been extended for dual-point design. The LVA was used to find an optimum airfoil in the design space of intermediate airfoils. Some design examples were presented with successful results. The computational load was much smaller than that of multipoint design methods using direct numerical optimization.

Some modification can be made to target pressure optimization code. To consider viscous drag component, boundary-layer calculation can be included in the target optimization code with the cost of computational time.

The extension of the present multipoint design method to three-dimensional wing design problems is straightforward and in progress.

References

[1]Hager, J. O., Eyi, S., and Lee, K. D., "Two-Point Transonic Airfoil Design Using Optimization for Improved Off-Design Performance," *Journal of Aircraft*, Vol. 31, No. 5, 1994, pp. 1143–1147.

[2]Mineck, R. E., Campbell, R. L., and Allison, D. O., "Application of Two Procedures for Dual-Point Design of Transonic Airfoils," NASA TP-3466, Sept. 1994.

[3]Santos, L. C., and Sankar, L. N., "A Hybrid Inverse Optimization Method for the Aerodynamic Design of Lifting Surfaces," AIAA Paper 94-1895, June 1994.

[4]Kim, H. J., and Rho, O. H., "Transonic Airfoil Design Using the Hybrid Inverse Optimization Method," International Symposium on Aeronautical Science and Technology in Indonesia, 96-1-2-1, Jakarta, Indonesia, June 1996.

[5]Michalewicz, Z., *Genetic Algorithms + Data Structures = Evolution Programs*, Springer–Verlag, New York, 1992.

[6]Hwang, S. W., "Numerical Analysis of Unsteady Supersonic Flow over Double Cavity," Ph.D. Dissertation, Seoul National Univ., Seoul, Republic of Korea, 1996.

[7]Cook, P. H., Mcdonald, M. A., and Firmin, M. C. O., "Aerofoil RAE2822-Pressure Distribution, and Boundary Layer and Wake Measurements," AGARD AR 138, May 1979, A6-1–A6-77.

[8]Johnston, L. J., "Solution of the Reynolds-Averaged Navier-Stokes Equations for Transonic Aerofoil Flows," *Aeronautical Journal*, Vol. 95, Oct. 1991, pp. 253–273.

[9]Malone, J. B., Narramore, J. C., and Sankar, L. N., "Airfoil Design Method Using the Navier-Stokes Equations," *Journal of Aircraft*, Vol. 28, No. 3, 1991, pp. 216–224.

[10]Press, W. H., Teukolsky, S. A., Vetterling, W. T., and Flannery, B. P., *Numerical Recipes in FORTRAN*, 2nd ed., Cambridge Univ. Press, Cambridge, England, UK, 1992, pp. 413–418.

[11]Van Egmond, J. A., "Numerical Optimization of Target Pressure Distributions for Subsonic and Transonic Airfoil Design," *Computational Methods for Aerodynamic Design (Inverse) and Optimization*, CP 463, AGARD, March 1990 (Paper 17).

[12]Mabey, D. G., "Physical Phenomena Associated with Unsteady Transonic Flows," *Unsteady Transonic Aerodynamics*, edited by D. Nixon, Vol. 120, Progress in Astronautics and Aeronautics," AIAA, Washington, DC, 1989, pp. 1–55.

[13]Harris, C. D., "NASA Supercritical Airfoils—A Matrix of Family-Related Airfoils," NASA TP-2969, March 1990.

[14]Campbell, R. L., "An Approach to Constrained Aerodynamic Design with Application to Airfoil," NASA TP-3260, Sept. 1992.